Fluorogenic dimers as bright switchable probes for enhanced super-resolution imaging of cell membranes

Ilya O. Aparin,[1,‡] Rui Yan,[2,3,‡] Rémi Pelletier,[1] Alexander A. Choi,[2,3] Dmytro I. Danylchuk,[1] Ke Xu, [2,3,*] Andrey S. Klymchenko[1,*]

[1] Laboratoire de Bioimagerie et Pathologies, UMR 7021 CNRS, Université de Strasbourg, 74 route du Rhin, 67401, Illkirch, France

[2] Department of Chemistry, University of California, Berkeley, Berkeley, California, 94720, United States

[3] Chan Zuckerberg Biohub, San Francisco, CA 94158, United States.

Abstract:

Super-resolution fluorescence imaging based on single-molecule localization microscopy (SMLM) enables visualizing cellular structures with nanometric precision. However, its spatial and temporal resolution largely relies on the brightness of ON/OFF switchable fluorescent dyes. Moreover, in cell plasma membranes the single-molecule localization is hampered by the fast lateral diffusion of membrane probes. Here, to address these two fundamental problems, we propose a concept of ON/OFF switchable probes for SMLM based on fluorogenic dimers of bright cyanine dyes. In these probes, the two cyanine units connected with a linker were modified at their extremities with low-affinity membrane anchors. Being self-quenched in water due to intramolecular dye H-aggregation, they displayed light up in apolar and viscous media, including lipid membranes. Charged group in the linker further decreased the probe affinity to the lipid membranes, thus accelerating its dynamic reversible ON/OFF switching. The concept was validated on red cyanine 3 and far-red cyanine 5 dyes. SMLM of live cells revealed that the new probes provided higher brightness and ~10-fold slower diffusion at the cell surface, compared to reference probes Nile Red and DiD, which boosted axial localization precision of biomembrane imaging >3-fold down to 31 nm. The new probe allowed unprecedented observation of nanoscale fibrous protrusions on plasma membranes of live cells with 40-s time resolution, revealing their fast dynamics. Thus, going beyond the brightness limit of single switchable dyes, using cooperative de-quenching in fluorogenic dimers, and slowing down probe diffusion in biomembranes open the route to significant enhancement of super-resolution fluorescence microscopy of live cells.

INTRODUCTION

A breakthrough discovery of super-resolution fluorescence microscopy allowed going beyond the diffraction limit and reaching nanoscale accuracy of cellular compartments in fluorescence imaging.[1-5] In particular, rapidly growing single-molecule localization microscopy (SMLM) techniques are capable of imaging single fluorescent (bio)molecules in cells below the diffraction limit.[2,6,7] However, the performance of SMLM relies on the quality of contrast agents – fluorescent molecular probes.[8-11]

Indeed, the resolution of SMLM methods is directly linked to the number of photons collected from single fluorescent molecules and the number of ON/OFF switching events registered during the image acquisition. During the past two decades, chemical engineering of fluorescent probes for SMLM at the cellular level underwent a significant progress.[8,9] To achieve robust ON/OFF switching for SMLM, a number of chemical and photochemical approaches have been followed:[12] (*i*) reactions of nucleophiles, such as thiols, with cyanine or xanthene derivatives;[13,14] (*ii*) spiro-lactonization in rhodamines and silicon-rhodamines,[15] or spirocyclization of their hydroxymethyl analogues (HIDE);[16,17] (*iii*) photo-induced isomerization resulting in reversible photoswitching;[18-20] (*iv*) dye exchange through DNA hybridization;[21,22] (*v*) charge transfer in solvatochromic dyes (e.g., Nile Red);[23-27] (*vi*) ground and excited state rotation in rotors (BODIPY)[28] and flippers.[29] In the latter two cases, reversible binding to apolar and rigid sites leads to a fluorescence light up. However, all these approaches are based on the use of a single fluorophore, which is characterized by physically limited brightness. To go beyond this limitation, design of ON/OFF switchable dye dimers is particularly attractive, as it allows direct multiplication of the signal by two using bright fluorescent dyes. Previous works introduced fluorogenic dimers of cyanines, squaraines and rhodamines that are self-quenched in water due to formation of H-aggregates and then light up after binding to their target such as nucleic acids[30-32] and membrane receptors.[33-35] However, the fluorogenic dimers have not been explored in SMLM so far.

SMLM that exploits ON/OFF switching of dyes due to reversible target binding is called points accumulation for imaging in nanoscale topography (PAINT).[23] Generally, it uses environment-sensitive dyes,[36] particularly Nile Red, which light up on binding to lipid membranes.[23-25,37] However, when non-fluorogenic dyes are used, for instance in DNA-PAINT,[21,22] the dye concentration is kept low to decrease the background, which leads to slower ON/OFF switching processes. The key advantage of PAINT is that it does not require specific agents to induce dye blinking, which can be toxic to cells, or complex multi-color excitation protocols, while providing relatively good spatial and temporal resolution. Moreover, PAINT uses a practically unlimited reservoir of probes in solution, so it is not affected by dye photobleaching, unlike other SMLM techniques. PAINT imaging with higher selectivity can be achieved by a rational design of the anchor group of Nile Red, which allows specific targeting of the outer leaflet of the plasma membranes.[27] PAINT technique can help to visualize nanoscale organization of lipid membranes,[24,25,27] especially the presence of lipid microdomains, which have been a matter of intense debates for decades.[38-40] Nevertheless, current environment-sensitive dyes are characterized by limited brightness and photostability. Another limitation is related to the fast diffusion of small molecular probes in biomembranes, with typical diffusion coefficients in the range between 1 and 15 $\mu m^2/s$, dependent on the method and the molecule used.[28,41-44] This fast probe diffusion decreases localization precision in biomembranes[44] and makes three-dimensional (3D) imaging[6] particularly challenging. Overall, new advanced probes for plasma membranes are urgently needed to further improve current super-resolution techniques.

Here, we propose to exploit the opening/closing of fluorogenic dimer as a mechanism to achieve reversible ON/OFF switching of dyes in PAINT super-resolution imaging while also substantially reducing the in-membrane diffusion. The concept addresses the problems of limited brightness of current fluorogenic dyes and their lateral diffusion in the plasma membrane, allowing enhanced spatial and temporal resolution of biomembrane imaging.

RESULTS AND DISCUSSION

The design of the fluorogenic dimer for plasma membranes is based on cyanine dyes, which are prone to self-quenching by H-aggregate formation, whereas disrupting the pi-stacking leads to their fluorescence light up.[45] The two identical cyanine dyes are connected by a spacer, while the extremities of the dimer are functionalized with negatively charged anchor groups (Figure 1a). The latter compensates the positive charge of the cyanine dyes and ensures low-affinity reversible binding to the cell plasma membrane. We expect that the designed dimeric probes are self-quenched in aqueous solution, while dynamic binding to cell membrane would open up the dimer leading to continuous ON/OFF switching, required for PAINT imaging. Initially, we designed dimer probes based on Cy3 dye (Figure 1a). As a membrane anchor attached at the probe extremities, we used a sulfonate group and short butyl chain (Figure 1b), which were previously reported to provide Nile Red with low affinity but high selectivity to the plasma membranes.[27] Two probes with different linkers were designed: (i) neutral cadaverine linker for **BTF-1** and (ii) anionic lysine linker for **BTF-2**. One should note that in both designed probes the linker length of five carbons was chosen, because, according to the previous works on fluorogenic dimers for imaging biomolecules, this length was optimal to obtain efficient self-quenched H-aggregates for rhodamine[31] and squaraine[34] dyes. First, the neutral **BTF-1** probe bearing a cadaverine linker was synthesized (Figure 1b). Starting from Cy3 diacid, it was turned into an asymmetric Cy3 derivative (**I**) by reaction with 3-(butylamino)propane-1-sulfonic acid.[27] Next, Cy3 (**I**) carboxylic acid was coupled with cadaverine using PyBOP, affording **BTF-1** with good yield after reverse phase-chromatography purification.

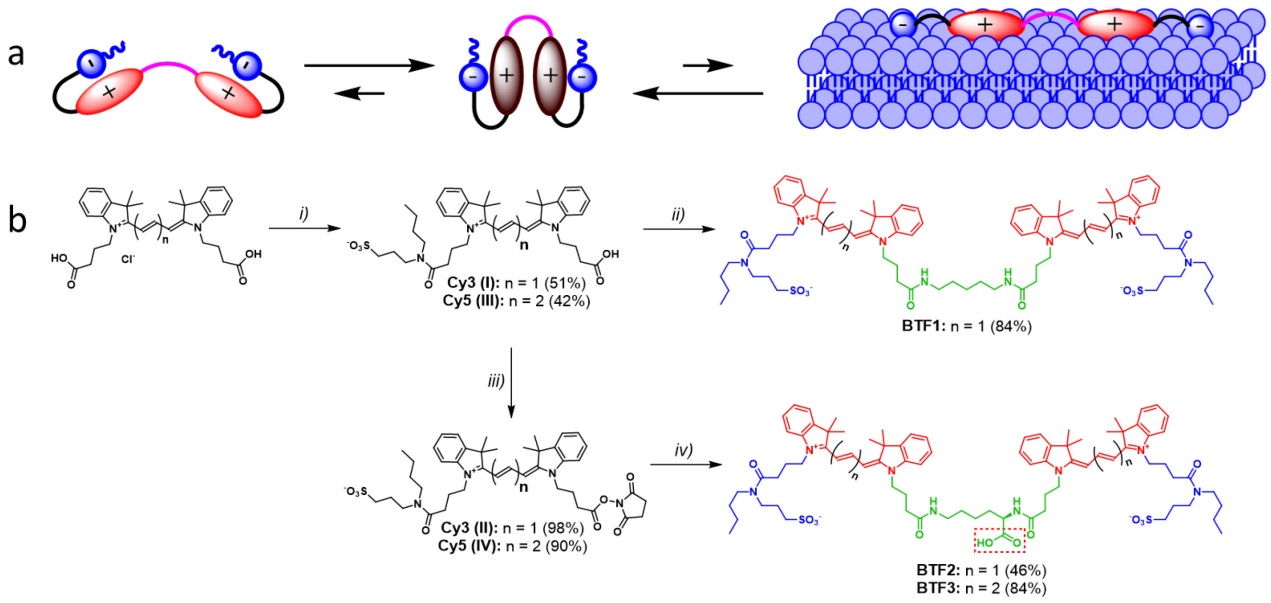

Figure 1. a) Concept of switchable cyanine-based dimeric probe that lights up after reversible binding to biomembranes. b) Synthetic scheme for Cy3-based **BTF-1**, **BTF-2** and Cy5-based **BTF-3** probes. Red rectangle highlights polar carboxylic group. Conditions: *i)* 3-(butylamino)propane-1-sulfonic acid, PyBOP, DIPEA, DMF; *ii)* cadaverine, PyBOP, DIPEA, DMF; *iii)* TSTU, DMF; iv) L-lysine, 0.2 M TEAA buffer (pH 8.25), DMF.

In order to adjust hydrophobic/hydrophilic balance of the probe, which eventually has a straightforward impact on its membrane affinity and ON/OFF turnover, **BTF-2** probe bearing an

additional carboxylic group within the L-lysine linker was designed. This group was expected to further reduce probe affinity to the plasma membrane and provide the probe a net negative charge. Avoiding additional protection/deprotection steps, **BTF-2** was obtained by direct L-lysine acylation with Cy3 NHS ester (**II**) in TEAA buffer/DMF 1:1 mixture. To this end, cyanine dye (**I**) was activated with TSTU reagent to obtain NHS ester (**II**) with quantitative yield, which was used without any purification in the next step. Poor lysine solubility in aprotic organic solvents necessitated the coupling stage in an aqueous-organic mixture, i.e. basic TEAA buffer with DMF. The obtained **BTF-2** was purified by a reversed-phase C18-silica column chromatography to reach 98+% purity by HPLC.

Next, we characterized the photophysical properties of **BTF-1** and **BTF-2** probes in comparison to a monomeric Cy3 (**I**) (Figure 2, Table 1). Monomeric Cy3 (**I**) exhibited classical absorption band in PBS, similar to that in organic solvents such as ethanol and glycerol (Figure 2a, S1). In contrast, absorption spectra of **BTF-1** and **BTF-2** measured in PBS (pH 7.4) displayed a short-wavelength band, characteristic of H-aggregates in different dimeric dyes.[31,33-35] For both probes the absorbance ratio of the short- to long-wavelengths I_S/I_L was ~1 in PBS vs 0.63-0.66 in organic solvents, whereas for the monomer Cy3 (**I**) it was similarly low (0.59) for PBS and organic solvents (Table 1). Since no pronounced scattering or band broadening were observed in the absorbance spectra, the nature of the H-aggregated state can be interpreted as a monomolecular dimer formation, rather than an intermolecular aggregation process. Remarkably, the characteristic short-wavelength band of the H-aggregate was present in the absorption spectra of **BTF-1** and **BTF-2**, independently of their concentration in the range 0.02 – 2 μM (Figure S2, S2), which confirmed the intramolecular nature of the H-aggregate. Fluorescence intensity and corresponding quantum yield (QY) of **BTF-1** and **BTF-2** were significantly lower in PBS compared to the monomer, in line with the significant fraction of self-quenched aggregates in solution (Figure 2b, S3-S4, Table 1). In organic solvents, the fluorescence QY of dimer and monomer dyes was similar, indicating that the H-aggregates of **BTF-1** and **BTF-2** were broken, and they emitted as monomeric species. As a result, the fluorescence enhancement was significantly higher for the dimers vs monomer, which is important for their further application as ON/OFF switchable probes. Additionally, all three compounds displayed strong fluorescence enhancement in viscous glycerol medium *vs.* phosphate saline buffer and ethanol (Figure 2b,c, Table 1). This effect is known for cyanine dyes[44] and associated with restriction in viscous medium of polymethine chain rotation and photoisomerization. We also studied the binding of the probes to model lipid membranes, 1,2-Dioleoyl-sn-glycero-3-phosphocholine (DOPC) liposomes, at different concentrations (Figure 2d, S5). Probes **BTF-1** and **BTF-2** showed gradual fluorescence increase with an increase in the lipid concentration up to 1000 nM without saturation. Importantly, for the more hydrophilic **BTF-2** this increase was slower, suggesting its lower affinity to the lipid membranes. The increase in the fluorescence intensity of the dimers was accompanied by the disappearance of the short-wavelength shoulder (Figure S6), which confirmed that the binding to the lipid vesicles let to the disruption of the H-aggregates of the probes (Figure 1a). In contrast, Cy3 (**I**) dye displayed a rapid increase in the fluorescence intensity at low concentrations of DOPC (<50 nM) with saturation behavior, indicating much higher affinity to the membranes compared to the dimers. Moreover, fluorescence enhancement for Cy3 (**I**) was much lower compared to the other two probes because of relatively strong emission in the aqueous buffer. Thus, the dimers exhibited high fluorogenic response on binding to lipid membranes, clearly due to the disruption of the H-aggregates, and low affinity to lipid membranes required to reversible binding, as schematized in Figure 1a.

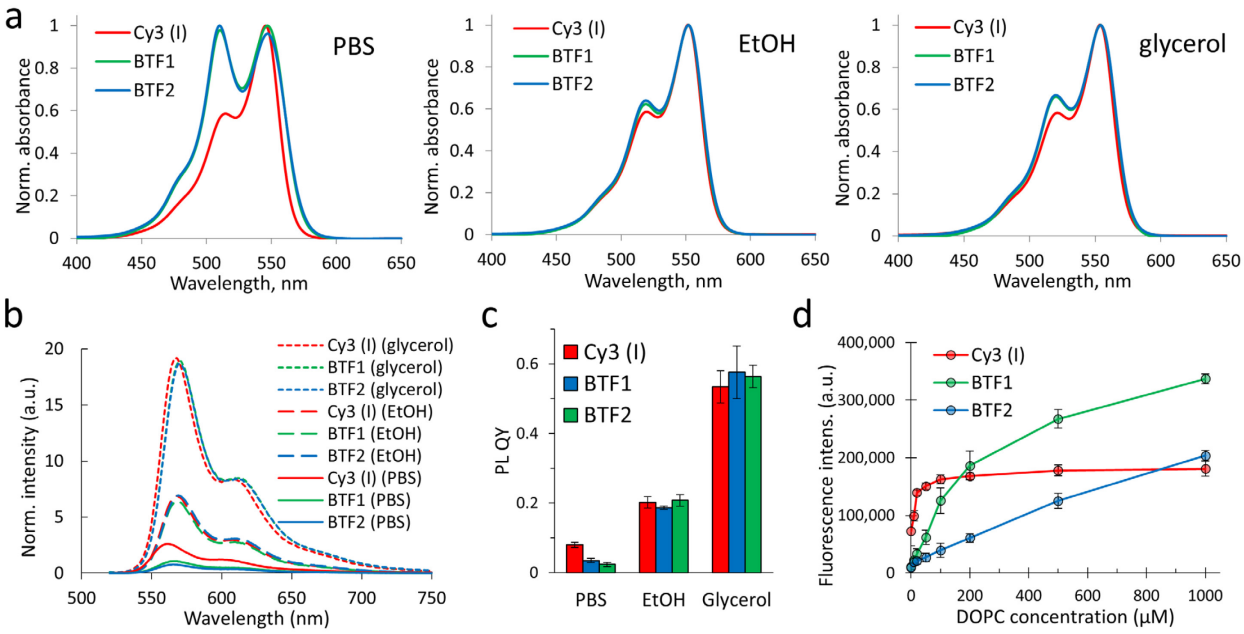

Figure 2. Photophysical characterization of the probes **BTF-1**, **BTF-2** and monomeric Cy3 (**I**). (a) Normalized absorption spectra measured at 4, 2 and 2 μM, correspondingly. (b) Fluorescence spectra of **BTF-1, BTF-2 and** Cy3 (**I**) at 0.2 μM, 0.2 μM and 0.4 μM, respectively, measured in PBS, ethanol, and glycerol. (c) Fluorescence quantum yields. (d) Titration of **BTF-1** and **BTF-2** (100 nM) and Cy3 (**I**) (200 nM) with increasing concentrations of DOPC lipid vesicles (phosphate buffer, pH 7.4): peak fluorescence intensity, excitation at 510 nm.

Table 1. Photophysical properties of **BTF-1**, **BTF-2** probes and monomer dye Cy3 (**I**).

Probe	Solvent	ε, ($M^{-1}cm^{-1}$)[a]	$\lambda_{abs}/\lambda_{emis}$, (nm)	I_S/I_L[b]	SBR[c]	QY, (%)[d]
Cy3(I)	PBS	143000	545/561	0.598	-//-	8.0±0.7
	Ethanol	152000	552/568	0.585	2.52	20.2±1.6
	Glycerol	142000	554/568	0.585	6.69	53.4±4.6
BTF-1	PBS	116000	547/568	0.980	-//-	3.5±0.6
	Ethanol	234000	552/568	0.625	5.31	18.6±0.5
	Glycerol	208000	554/570	0.662	16.40	57.6±7.6
BTF-2	PBS	120000	547/565	1.04	-//-	2.3±0.6
	Ethanol	218000	552/569	0.641	8.90	20.8±1.7
	Glycerol	196000	554/569	0.667	24.12	56.3±3.3

a) determined at λ_{max} for each solvent; *b)* absorptivity ratio for H-aggregate and free dye forms, determined at λ_{max} for fluorophore (I_L) and its H-aggregated forms (I_S); *c)* SBR = QY_{solv}/QY_{PBS}; *d)* with respect to rhodamine B in ethanol as a standard (QY 65%), excitation wavelength: 510 nm.

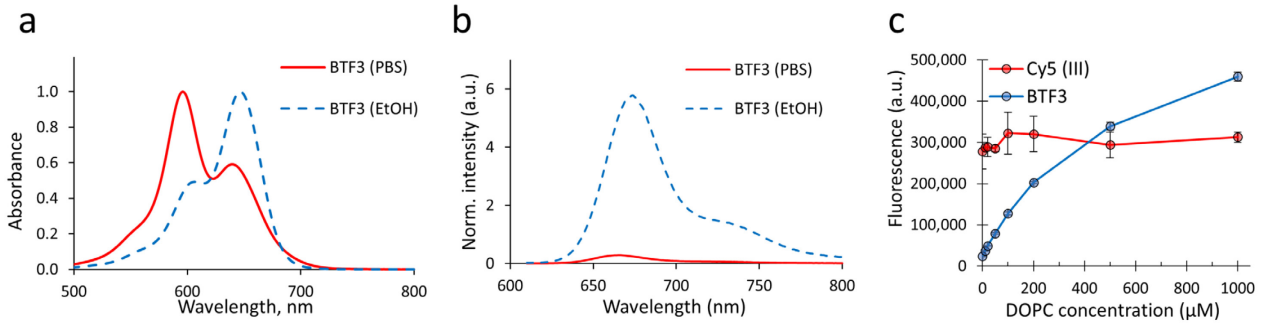

Figure 3. Absorption (a) and fluorescence (b) spectra of **BTF-3** in different media measured at 0.2 μM concentration. Excitation wavelength: 600 nm. Fluorescence spectra are normalized with respect to absorptivity at 600 nm. (c) Titration of **BTF-3** (100 nM) and Cy5 (III) (200 nM) with increasing concentrations of DOPC lipid vesicles (phosphate buffer, pH 7.4): peak fluorescence intensity, excitation at 600 nm.

Given promising results obtained with Cy3-based dimers in solvents and lipid vesicles, we explored the applicability of the dimer design to the red-shifted Cy5 dye. As the spectroscopy data revealed better performance for **BTF-2** probe vs. **BTF-1**, the lysine spacer was chosen to develop Cy5-based dimer **BTF-3** (Figure 1b). Following the developed protocol for **BTF-2**, Cy5 diacid was mono-derivatized with 3-(butylamino)propane-1-sulfonate to afford zwitterionic Cy5 (**III**) mono-carboxylic acid. Next, Cy5 (**III**) was activated with TSTU and immediately used in the next step for **BTF-3** synthesis, based on the methodology mentioned above for **BTF-2**. To facilitate and simplify purification, **BTF-3** was separated by size-exclusion chromatography on LH-20 Sephadex with a high yield (84%) and good purity.

In organic solvents ethanol and glycerol, the absorption spectrum of **BTF-3** showed maximum around 650 nm (Figure 3a), which is close to its monomer analogue Cy5 (III) (Figure S7). In contrast, in PBS a characteristic short-wavelength absorption band was observed for **BTF-3**, which can be assigned to the H-aggregate of the dimer. Remarkably, in this dimer the contribution of H-aggregate band was higher compared to that in the Cy3 analogue **BTF-2** (Figure 2a and 3a). We could speculate that the larger pi-conjugated flat structure of Cy5 with its slightly higher hydrophobicity compared to Cy3 favors more efficient H-aggregation driven by pi-staking in water. Importantly, the band of H-aggregate did not show significant variations at the large range of concentrations (20-2000 nM, Figure S8), which confirmed the intramolecular nature of the H-aggregate. The control compound Cy5 (III) did not show any significant variations in the absorption spectra for the three studied media (Figure S7), which was expected for a monomeric dye. The fluorescence intensity of **BTF-3** in PBS was much weaker compared to that in organic solvents (Figure 3b) and this tendency was observed by strong variations in the QY values (Table S1). Thus, the dimeric dye **BTF-3**, similarly Cy3 analogue **BTF-2**, shows fluorogenic response (turn-on) in organic solvents vs aqueous PBS, which is linked to the disruption of its H-aggregate provoked by solvation of its Cy5 units. Addition of lipid vesicles to the PBS solution of **BTF-3** led to a gradual fluorescence enhancement (Figure 3c), suggesting that the dye binds to lipid bilayers and light up its fluorescence. This light up was also accompanied by the loss of short-wavelength band of the H-aggregate (Figure S6). The fact that the binding curve did not show saturation even at 1000 μM indicated that the affinity of this dimer remains relatively low, so that its behavior is similar to that of **BTF-2**. In contrast, the monomeric analogue Cy5 (III) did not show any fluorescence enhancement in the presence of lipid vesicles, which was expected because of

lack in the fluorogenic character of this dye. Thus, we conclude that our dimeric design can be applied to different cyanine dyes, yielding fluorogenic dyes with different colors.

We next examined the performance of **BTF-1** and **BTF-2** in PAINT microscopy of live cells. By simply adding the probes into the cell medium at ~4 nM, without any washing steps, we observed excellent single-molecule fluorescence ON/OFF switching in the plasma membrane under the typical ~1 kW/cm^2 560 nm illumination and wide-field recording at the typical framerate of 110 frame per second (fps) (Figure 4a,b and Movie S1). The concentration was optimized to avoid the overlapping of single-molecule images for reliable 3D-SMLM and at the same time ensure fast binding-unbinding processes required for PAINT. The spontaneous switching maintained a good density of single molecules over long periods through the medium-cell membrane dye exchange. Examination of single-molecule trajectories indicated that ~40% of the detected molecules only showed up in one frame, while most lasted 1-3 frames (Figure S31). Intensity time traces for the occasionally observed long (>50 frames) trajectories showed rare events of stepwise photobleaching (Figure S31), suggesting that the typical short (<3 frames) duration of single-molecule emission was mostly due to unbinding from the membrane. The count of detected molecules did not drop significantly over ~100,000 frames of continuous recording (Figure 4d), during which process ~5×10^6 molecules were detected. The frequencies of the ON/OFF events for **BTF-2** were significantly higher than for **BTF-1** (Figure 4d), because the lower affinity of the former to lipid membranes (Figure 2d) favors faster binding/unbinding dynamics. Indeed, as it was shown previously for Nile Red derivatives, the probe with lower affinity exhibited faster localization counts compared to the high-affinity probe, which was linked to faster probe unbinding and thus turnover on the membrane.[27]

Both **BTF-2** and **BTF-1** generated excellent single-molecule images with high brightness, low background, and well-defined shapes. A direct comparison with Nile Red, one of the most used dyes in PAINT microscopy,[23-25,37] highlighted the superior performances of **BTF-2** and **BTF-1** (Figure 4c and Movie S1). Both dyes emitted >2-fold more photons for the detected single molecules in each recorded frame under typical SMLM conditions (Figure 4e), and we further found that BTF-2 consistently yielded substantially brighter single molecules than Nile Red under different illumination powers. These results are expected given the much higher extinction coefficients of **BTF-2** and **BTF-1** (Table 1) than Nile Red (ε~38,000 M^{-1}cm^{-1}).[46,47]

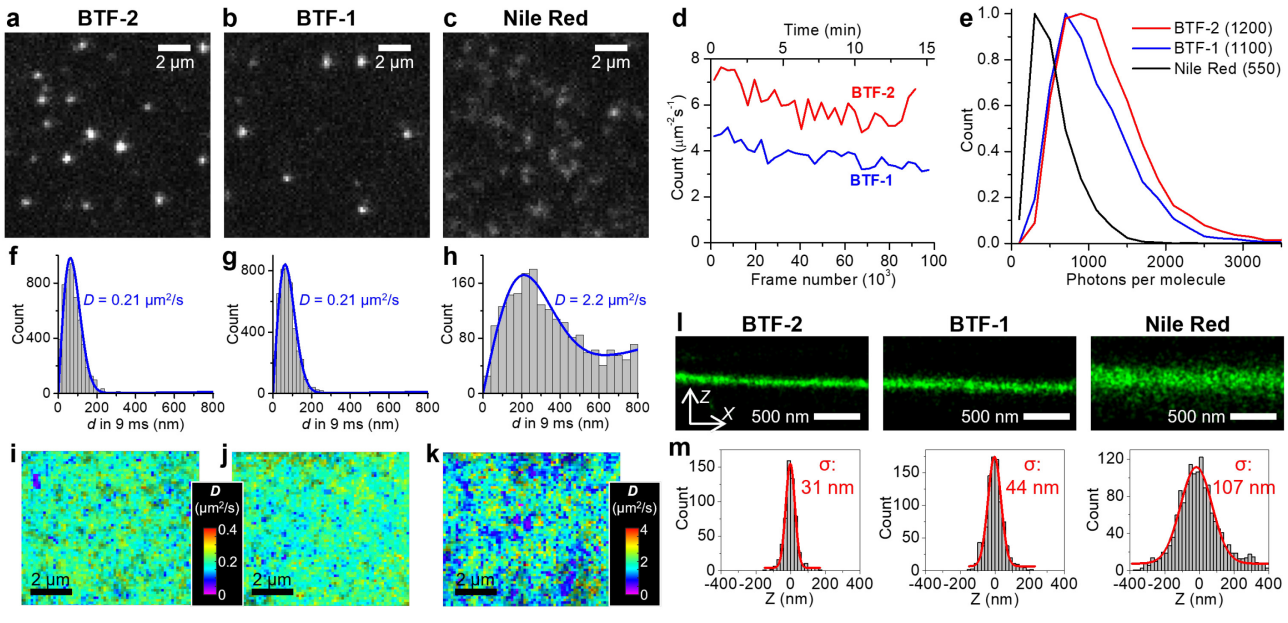

Figure 4. Single-molecule and 3D-PAINT characterizations of **BTF-1** and **BTF-2** in comparison to Nile Red. (a-c) Representative frames of single-molecule images of **BTF-2** (a), **BTF-1** (b), and Nile Red (c) in the plasma membrane of a live COS-7 cell, under continuous 560 nm illumination at ~1 kW/cm^2 and recorded at ~9 ms exposure time. (d) Time-dependent counts of detected **BTF-2** and **BTF-1** single molecules per second per μm^2 of membrane. (e) Distributions of the single-molecule photon counts recorded in each frame for the three dyes. (f-h) Typical distributions of single-molecule displacements in successive frames for the three dyes. Blue curves: fits to our model[48] to determine the diffusion coefficient *D*. (i-k) SM*d*M maps of local *D* for the three dyes. Note different *D* color scales. (l) Typical vertical cross-sections of the 3D-PAINT data of the three dyes at the plasma membrane. (m) Scattering in *Z* values for local flat regions. Gaussian fits (red curves) give standard deviations of 31, 44, and 107 nm, respectively.

Moreover, we found that the single-molecule images of **BTF-2** and **BTF-1** were characterized by substantially suppressed motion-blur. Under the typical ~110 fps recording framerate of modern EM-CCD camera, Nile Red showed markedly distorted and blurred single-molecule images as the molecules quickly tumbled in the membrane (Figure 4c and Movie S1). In contrast, the **BTF-2** and **BTF-1** single-molecule images exhibited little motion-blur and limited motion between frames (Figure 4ab and Movie S1). Statistics of the single-molecule displacement in successive frames showed drastic differences (Figure 4f-h). Fitting to a two-dimensional diffusion model[48] showed that whereas the intra-membrane diffusion coefficient *D* was ~2.2 μm^2/s for Nile Red, typical of membrane dyes,[28,43,44] the corresponding values were ~0.2 μm^2/s for **BTF-2** and **BTF-1**. Spatially gridding the displacements for local fitting and hence single-molecule displacement/diffusivity mapping (SM*d*M)[28,48] generated super-resolution maps of *D* that showed consistent drops in diffusivity of the dimers by one order of magnitude (Figure 4i-k; note different color scales). This slow diffusion may be attributed to the dimeric structure of the probes with a high length of the molecule in the open form (45 atoms between the sulfonate head groups, Figure 1), which could drastically complicate the lateral motion of the probe within the biomembrane, composed of both lipids and proteins.

The combined advantages of higher brightness and reduced motion-blur for **BTF-2** and **BTF-1** enabled outstanding resolution in 3D-PAINT microscopy, based on a cylindrical lens method.[6] In this method, the single-molecule image shape is converted into the depth (*Z*) values, so that motion-blur quickly degrade the *Z* resolution. Although the single-molecule motion-blur may be reduced via stroboscopic excitation,[28,49] dedicated hardware and higher laser powers are required. Here, under continuous illumination and the typical 110 fps framerate, we examined vertical cross-sections of the 3D-PAINT data obtained with the three probes for flat parts of the cell membrane (Figure 4l). **BTF-2** and **BTF-1** showed much sharper images, with localization precision in *Z* reaching 31 and 44 nm, respectively (Figure 4m), substantially superior to that obtained with the reference probe Nile Red (107 nm). Additionally, whereas we have recently reported BDP-TMR-alkyne as being similarly bright as **BTF-2** and **BTF-1** in single-molecule emission, its fast diffusion at >2 μm^2/s limited the achievable SMLM localization precision in *Z* to ~80 nm under comparable experimental conditions, and it further exhibited a strong non-specificity in labeling intracellular membranes.[28]

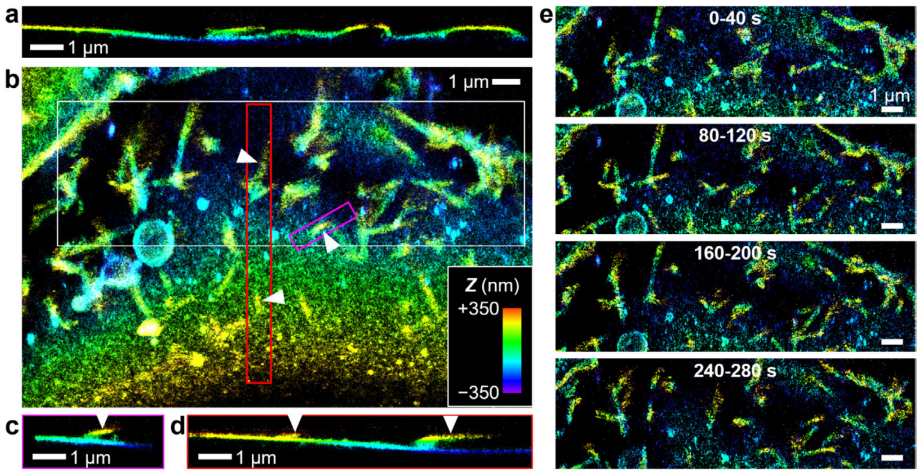

Figure 5. 3D-PAINT with **BTF-2** unveils rich 3D structures and dynamics of the plasma membrane in living cells. The sample was continuously illuminated with 560 nm at ~1 kW/cm^2 in the wide field and recorded at 110 frames per second with an ~9 ms exposure time. (a) Vertical cross-sectional view of the 3D-PAINT data of the plasma membrane of a COS-7 cell with undulating membrane heights. (b) In-plane view of another cell, highlighting numerous nanoscale tubules. (c,d) Vertical cross-sectional views along the magenta (c) and red (d) boxes in (b), showing tubules protruding away from the cell surface (arrowheads). Note that in the vertical cross-sectional views shown in (a,c,d), the vertical dimension corresponds to depth into the sample. (e) Time-divided 3D-PAINT data in 40 s brackets at 4 time points, for the white box in (b). See Movie S2 for the full sequence. For all images, color presents depth (*Z*) according to the color scale in (b).

Leveraging the above high resolution and specificity to the plasma membrane, we examined the 3D structure of the dorsal membrane of living COS-7 cells using **BTF-2**. Notably, besides observing membrane height undulations (Figure 5a), we unveiled numerous thin tubules (Figure 5b), with vertical cross-sections visualizing their protrusion away from the cell surface (Figure 5c,d). With typical widths of ~100 nm and lengths of ~1 μm, these small structures would otherwise be difficult to resolve without plasma-membrane-specific labeling and high imaging resolution. A recent SMLM study resolved similar tubules in fixed cells through covalent labeling of the membrane surface glycocalyx.[50] However, specialized labeling chemistry was required, and the strategy may be difficult to apply to live cells. With **BTF-2**, we readily resolved the tubules after simply adding the dye to the cell medium. Moreover, by working with the living cell, we unveiled the fast-reshaping dynamics of these nanoscale tubules with sub-minute time resolutions (Figure 5e and Movie S2). These results suggest that the plasma membrane is far from a static, isotropic flat sheet, but is characterized by dynamic heterogeneities at the nanoscale. Such spatiotemporal heterogeneities may regulate how the cell interacts with its environments, while also calling for cautions in designing and interpreting macroscale measurements of cell membrane properties.

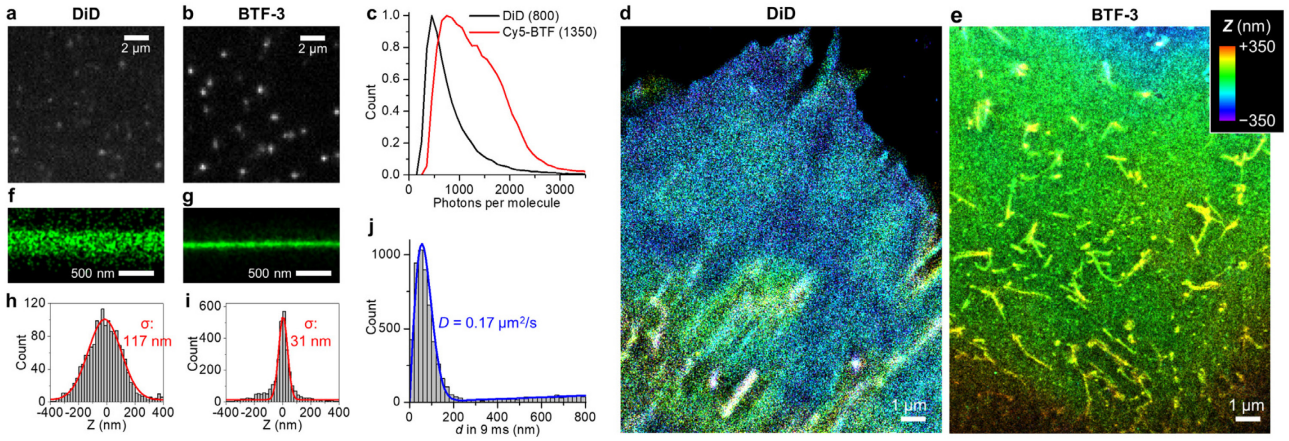

Figure 6. Single-molecule and 3D-PAINT characterizations of **BTF-3** in comparison to the Cy5-based DiD dye. (a,b) Representative frames of single-molecule images of DiD (a) and **BTF-3** (b) in the plasma membrane of a live COS-7 cell, under continuous 647 nm illumination at ~1 kW/cm^2 and recorded at 110 frames per second with an ~9 ms exposure time. (c) Distributions of the single-molecule photon counts recorded in each frame for the two dyes. (d) Example 3D-PAINT images of DiD (d) and **BTF-3** (e) of the plasma membrane of live COS-7 cells. (f,g) Typical vertical cross-sections of the 3D-PAINT data of the two dyes at the plasma membrane. (h,i) Spread in Z values for local flat regions. Gaussian fits (red curves) give standard deviations of 117 and 31 nm, respectively. (j) Typical distributions of single-molecule displacements in successive frames for **BTF-3**. Blue curve: fits to our model,[48] yielding a diffusion coefficient D of 0.17 um^2/s.

Finally, we tested Cy5-derivative **BTF-3** and directly compared it to a reference Cy5-based monomeric probe DiD previously used in the SMLM of cell membranes.[44] Under typical continuous 647 nm SMLM illumination at ~1 kW/cm^2 in the wide field, both dyes exhibited single-molecule blinking (Movie S3). However, **BTF-3** was notably brighter (Figure 6a,b and Movie S3), with single-molecule analysis showing an ~70% higher photon count when compared to that of DiD (Figure 6c). 3D-PAINT microscopy showed clear advantage of **BTF-3** compared to DiD in terms of the image resolution (Figure 6d,e). In the better resolved images of plasma membrane of COS-7 cells, one could observe diverse nanoscopic structures (Figure 6e), similar to those revealed by probe **BTF-2** (Figure 5b). The achieved Z-localization precision of **BTF-3** of 31 nm was similar to that of **BTF-2**, being much better compared to that of DiD (117 nm, Figure 6f-i). Analysis of single-molecule displacement revealed a remarkably low diffusion coefficient of 0.17 µm^2/s for **BTF-3** (Figure 6j). This result confirms that our dimer-based design inhibits dye diffusion on the membrane and ensures much better performance of **BTF-3** in super-resolution imaging of plasma membranes compared to monomeric dye DiD.

CONCLUSIONS

In conclusion, this work addresses the fundamental drawbacks of fluorogenic dyes used in super-resolution (PAINT) microscopy of cell membranes: low brightness and fast lateral diffusion in biomembranes. We designed fluorogenic dimers that undergo reversible ON/OFF switching of bright fluorophores simultaneously on binding to the cell membranes. The probes are composed of two

identical cyanine dyes (red dye Cy3 or far-red dye Cy5) connected by a linker (cadaverine or lysine), modified at extremities by two low-affinity membrane anchors. Spectroscopic studies show that both Cy3 and Cy5-based dimers undergo strong self-quenching in aqueous media and efficient light up in organic solvents and lipid vesicles. Owing to their fluorogenic character, both probes display spontaneous blinking in no-wash conditions using single molecule localization microscopy (PAINT). We also found that higher polarity of the linker connecting the two dyes, which decreases affinity to the membrane, accelerates membrane binding/unbinding turnover and thus improves resolution of PAINT microscopy. Both Cy3 and Cy5-based dimers exhibit higher single-molecule brightness compared to their reference probes Nile Red and DiD, respectively, as well as ~10-fold slower diffusion at the membrane surface. These two critical properties enable ~3-fold enhancement in the axial resolution of the single molecules localization microscopy (PAINT) of live cell membranes. Moreover, using the developed probes, real-time 3D observation of the dynamics of nanoscale protrusions at the cell surface at 40-s time resolution is achieved, which was not possible before with other fluorogenic dyes. In comparison to previously developed concepts of blinking at the membrane surface, including HIDE probe[16] and fluorogenic Nile Red[24,25] and its improved analogue,[27] the concept of fluorogenic dimers presents two key advantages: (i) two fluorophores provide higher single-molecule brightness and (ii) dimeric design provides much slower diffusion at the membrane, which suppresses the motion-blur effects in single-molecule imaging. Regarding potential limitations of the new approach, one should mention non-negligible fluorescence in the aqueous solution and some absorbance at the excitation wavelength used, which could be a source of background and photo-bleaching in the medium. Overall, our work shows that exploiting cooperative de-quenching phenomena in multimeric dyes opens the way beyond the brightness limits of single fluorophores. Moreover, controlling dye diffusion in the biomembrane is also a key factor that can further enhance the performance of super-resolution imaging. As the fluorogenic dimers can be designed from different dyes, including, squaraines,[35] BODIPY,[51] rhodamines[31] and even near-infrared cyanines,[33] the proposed design concept could yield a large variety of bright ON/OFF switchable probes of different color for super-resolution imaging.

EXPERIMENTAL SECTION

General Methods and Materials. All the reagents were purchased from Sigma-Aldrich, Alfa Aesar or TCI and used without any purification. Cy3 and Cy5 diacids[52] and 3-(butylammonio)propane-1-sulfonate[53] were synthesized as described previously. MilliQ-water (Millipore) was used in all experiments. NMR spectra were recorded on BrukerAvance III 400 spectrometer. Mass spectra were obtained using an Agilent Q-TOF 6520 mass spectrometer with electrospray ionization. HPLC analyses were performed on Agilent 1260 Infinity II system equipped with Interchim PF5C18AQ-250/046 reversed phase column with gradual eluting from eluent A to eluent B for 20min at 1 ml/min; eluent A : 50 mM triethylammonium acetate (pH 5.5) in miliQ water 90% and acetonitrile 10%; eluent B: pure acetonitrile. Absorption and emission spectra were recorded on Agilent Cary 5000 UV-Vis-NIR spectrophotometer and Edinburgh FS5 spectrofluorometer, correspondingly. Fluorescence quantum yields were measured using rhodamine B in ethanol as a reference (QY = 0.70) [54] and DiD in methanol (QY = 0.33)[55] for Cy3 and Cy5-based dyes, respectively. DOPC liposome solution in 20 mM phosphate buffer (pH 7.4) was prepared by using a Lipex Biomembranes extruder (Vancouver, Canada) as mentioned previously and diluted to the final concentration: 0, 10, 20, 50,

100, 200, 500, 1000 µM.[27] To these solutions Cy3 (**I**), **BTF-1** – **BTF-3** were added and gently agitated for 5 mins prior to fluorescence measurements.

3-(N-butyl-4-(2-((E)-3-((Z)-1-(3-carboxypropyl)-3,3-dimethylindolin-2-ylidene)prop-1-en-1-yl)-3,3-dimethyl-3H-indol-1-ium-1-yl)butanamido)propane-1-sulfonate (Cy3 (**I**) carboxylic acid).
Cyanine 3 diacid (305 mg, 0.53 mmol), 3-(butylammonio)propane-1-sulfonate (114 mg, 0.58 mmol), DIPEA (230 µL, 1.33 mmol) were dissolved in abs. DMF (2mL). The mixture was cooled with an ice bath and PyBOP (300 mg, 0.58 mmol) was added in one portion. Stirring was continued for 4 h allowing the temperature rising to room. Then reaction was quenched with water (1 mL) and concentrated in vacuum until viscous substance. The residue was triturated with diethyl ether (20 mL), filtered off and washed with ether. The mixture was applied onto a column with C18 reversed phase silica gel and separated by gradual elution with acetonitrile/miliQ water/acetic acid from 10:90:0.5 to 40:60:0.5 v/v/v %. The middle fraction of the mono-substituted product was concentrated in vacuum to obtain 182 mg (51%) of magenta bulk solid. R_f = 0.31 (DCM/MeOH/AcOH = 90:10:0.2); ^{1}H NMR (400.13 MHz, chloroform-d) δ ppm: 8.40 (t, *J* = 13.4 Hz, 1H), 7.40 (q, *J* = 7.4 Hz, 2H), 7.31-7.40 (m, 5H), 7.20-7.25 (m, 3H), 6.86 (d, *J* = 13.4 Hz, 1H), 6.79 (d, *J* = 13.4 Hz, 1H), 4.20 (m, 4H), 3.68 (m, 3 H), 3.32 (t, *J* = 7.4 Hz, 2H), 2.98 (m, 2H), 2.82 (t, *J* = 7.4 Hz, 2H), 2.70 (t, *J* = 6.8 Hz, 2H), 2.13 (m, 6H), 1.70 (2×s, 12H), 1.47 (m, 2H), 1.28 (tq, J_1 = 7.3 Hz, J_2 = 7.5 Hz, 2H), 0.88 (t, *J* = 7.3 Hz, 3H); ^{13}C NMR (100.61 MHz, chloroform-d) δ ppm: 174.58, 174.04, 173.66, 172.27, 150.87, 141.69, 141.67, 140.34, 129.00, 128.92, 125.40, 125.23, 121.94, 121.79, 111.58, 110.94, 104.00, 103.89, 49.07, 48.87, 47.74, 46.64, 45.62, 44.07, 43.49, 31.41, 30.14, 29.91, 28.04, 28.00, 25.01, 23.75, 22.94, 20.08, 13.76; HRMS (ESI) m/z: [M+H] calcd. for $C_{38}H_{52}N_3O_6S^+$: 678.3571, found: 678.3585.

3-(N-butyl-4-(2-((1E,3E)-5-((Z)-1-(3-carboxypropyl)-3,3-dimethylindolin-2-ylidene)penta-1,3-dien-1-yl)-3,3-dimethyl-3H-indol-1-ium-1-yl)butanamido)propane-1-sulfonate (**Cy5 (III)** carboxylic acid).
Cyanine 5 diacid (317 mg, 0.60 mmol), 3-(butylammonio)propane-1-sulfonate (129 mg, 0.66 mmol), DIPEA (263 µL, 1.50 mmol) were dissolved in abs. DMF (2mL). The mixture was cooled with an ice bath and PyBOP (342 mg, 0.66 mmol) was added in one portion. Stirring was continued for 4 h allowing the temperature rising to room. Then reaction was quenched with water (1 mL) and concentrated in vacuum until viscous substance. The residue was triturated with diethyl ether (20 mL), filtered off and washed with ether. The mixture was applied onto a column with C18 reversed phase silica gel and separated with gradual eluting with acetonitrile/miliQ water/acetic acid from 10:90:0.5 to 20:80:0.5 v/v/v %. The middle fraction of the mono-substituted product was concentrated in vacuum to obtain 177 mg (42%) of blue bulk solid. R_f = 0.35 (DCM/MeOH/AcOH = 90:10:0.2); ^{1}H NMR (400.13, MeOD) δ ppm: 8.25 (t, *J* = 13.0 Hz, 2H), 7.48 (t, *J* = 5.8 Hz, 2H), 7.31-7.44 (m, 4H), 7.21-7.30 (m, 2H), 6.68 (m, 1H), 6.40 (m, 2H), 4.17 (m, 4H), 3.52 (t, *J* = 7.7 Hz, 2 H), 3.37 (t, *J* = 7.7 Hz, 1H), 2.87 (q, *J* = 7.2 Hz, 2H), 2.65 (t, *J* = 6.9 Hz, 1H), 2.52 (m, 3H), 2.07 (m, 6H), 1.72 (s, 12H), 1.52 (m, 2H), 1.31 (m,4H), 0.93 (m, 3H); ^{13}C NMR (100.61 MHz, MeOD) δ ppm: 173.64, 173.56, 173.33, 173.17, 172.41, 172.38, 162.21, 154.41, 154.32, 154.14, 154.01, 142.16, 142.12, 142.09, 141.31, 141.29; 128.41, 128.34, 125.66, 125.61, 124.95, 124.90, 124.81, 124.76, 122.03, 121.99, 117.84, 115.51, 110.80, 110.72, 110.64, 110.54, 103.48, 103.21, 103.07, 102.90, 49.24, 49.13, 48.60, 48.47, 46.49, 45.63, 45.02, 43.20, 43.05, 42.91, 42.80, 30.52, 29.60, 29.34, 28.64, 26.62, 26.59, 26.55, 24.11, 23.12, 22.53, 22.29, 22.21, 19.87, 19.72, 12.90, 12.6; HRMS (ESI) m/z: [M+H] calcd. for $C_{40}H_{54}N_3O_6S^+$: 704.3722, found: 704.3722.

3-(N-butyl-4-(2-((E)-3-((Z)-1-(4-((2,5-dioxopyrrolidin-1-yl)oxy)-4-oxobutyl)-3,3-dimethylindolin-2-ylidene)prop-1-en-1-yl)-3,3-dimethyl-3H-indol-1-ium-1-yl)butanamido)propane-1-sulfonate (Cy3 NHS ester (**II**)).

Cyanine 3 free carboxylic acid (**I**) (68 mg, 0.1 mmol) was dissolved in dry DCM (1 mL) followed by DIPEA (26 µL, 0.15 mmol) and TSTU (45 mg, 0.15 mmol). The reaction was kept with stirring at room temperature for 5 h and precipitated with diethyl ether (20 mL) and acetic acid (100 µL) mixture. Formed solid was separated by filtration, washed with ether (2×10 mL) and dried in vacuum desiccator. NHS ester of Cy3 derivative (73 mg, 98%) was obtained as fine red powder and used in the next step without any intermediate purification. R_f = 0.43 (DCM/MeOH/AcOH = 90:10:0.2); ^{1}H NMR (400.13 MHz, chloroform-d) δ ppm: 8.42 (t, *J* = 13.4 Hz, 1H), 7.38 (m, 2H), 7.33 (d, J =7.4 Hz, 2H), 7.18-7.28 (m, 5H), 7.11 (d, *J* = 13.4 Hz, 1H), 4.38 (t, *J* = 7.9 Hz, 2H), 4.22 (t, *J* = 7.5 Hz, 2H), 3.71 (t, *J* = 8.2 Hz, 2H), 3.31 (t, *J* = 7.4 Hz, 2H), 3.14 (t, *J* = 6.8 Hz, 2H), 2.96 (t, *J* = 5.9 Hz, 2H), 2.77-2.86 (m, 6H), 2.24 (tt, J_1 = 7.8 Hz, J_2 = 6.9 Hz, 2H), 2.15 (m, 4H), 1.71 (s, 6H), 1.70 (s, 6H), 1.48 (m, 2H), 1.28 (m, 2H), 0.89 (t, *J* = 7.3 Hz, 3H); ^{13}C NMR (100.61 MHz, chloroform-d) δ ppm: 174.15, 173.69, 172.56, 169.13, 169.03, 151.41, 141.97, 141.84, 140.48, 140.43, 129.00, 128.96, 125.27, 125.09, 121.85, 121.80, 111.50, 111.10, 104.64, 49.00, 48.80, 47.89, 46.82, 45.60, 44.33, 43.01, 30.72, 30.02, 28.17, 28.12, 27.71, 25.58, 25.51, 24.37, 22.27, 20.12, 13.82; HRMS (ESI) m/z: [M+H] calcd. for $C_{42}H_{55}N_4O_8S^+$: 775.3735; found: 775.3740.

3,3'-((4,4'-(((1E,1'E)-((2Z,2'Z)-((pentane-1,5-diylbis(azanediyl))bis(4-oxobutane-4,1-diyl))bis(3,3-dimethylindoline-1-yl-2-ylidene))bis(prop-1-en-1-yl-3-ylidene))bis(3,3-dimethyl-3H-indole-1-ium-2,1-diyl))bis(butanoyl))bis(butylazanediyl))bis(propane-1-sulfonate) (**BTF-1**).

Cyanine 3 acid (I) (170 mg, 0.25 mmol) was dissolved in abs. DMF (1 mL) in flame-dried flask with a stir bar. DIPEA (53 µL, 0.3 mmol) was injected and the solution was cooled with an ice bath. PyBOP (140 mg, 0.27 mmol) was added in one portion and the reaction was stirred for 40 min followed by addition of cadaverine (14.0 µL, 0.12 mmol). Stirring was continued for another 4h allowing the temperature rise to room. Then water (100 µL) was added to quench reaction and homogeneous solution was precipitated with diethyl ether (30 mL) organic phase was decanted and the solid residue was applied onto the column with silica gel and gradually eluted with (DCM/MeOH/AcOH from 98:2:0.2 to 85:15:0.2). Magenta solid bulk 145 mg (84%) of Cy3 dimer (**BTF-1**) was obtained after concentration in vacuum. R_f = 0.23 (DCM/MeOH/AcOH = 90:10:0.2); ^{1}H NMR (400.13 MHz, chloroform-d) δ ppm: 8.40 (t, *J* = 13.4 Hz, 2H), 8.03 (t, *J* = 5.4 Hz, 2H), 7.32-7.40 (m, 8H),7.21-7.28 (m, 8H) 7.09 (d, *J* = 13.6 Hz, 2H), 6.97 (d, *J* = 13.4 Hz, 2H), 4.23 (m, 8H), 3.70 (t, *J* = 8.0 Hz, 4H), 3.34 (t, *J* = 7.5 Hz, 4H), 3.22 (dt, J_1 = 6.8 Hz, J_2 = 5.9 Hz, 4H), 2.98 (m, 4H), 2.84 (t, *J* = 7.4 Hz, 4H), 2.66 (t, *J* = 7.4 Hz, 4H), 2.15 (m, 12H), 1.71 (s, 12H), 1.70 (s, 12H), 1.46-1.60 (m, 8H), 1.41 (m, 2H), 1.29 (m, 4H), 0.90 (t, *J* = 7.3 Hz, 6H); ^{13}C NMR (100.61 MHz, chloroform-d) δ ppm: 173.99, 173.58, 172.88, 172.33, 151.11, 141.90, 141.86, 140.50, 140.36, 129.04, 128.97, 125.30, 125.10, 121.79, 121.76, 111.56, 111.36, 104.66, 104.04, 48.98, 48.91, 48.07, 46.92, 45.62, 44.06, 39.36, 33.36, 30.43, 30.06, 29.64, 28.92, 28.14, 28.06, 25.38, 24.36, 24.31, 24.15, 20.18, 13.86; HRMS (ESI) m/z: [M+2H]/2 calcd. for $C_{81}H_{114}N_8O_{10}S_2^{2+}$: 711.4044; found: 711.4016.

3,3'-((4,4'-(((1E,1'E)-((2Z,2'Z)-((((S)-1-carboxypentane-1,5-diyl)bis(azanediyl))bis(4-oxobutane-4,1-diyl))bis(3,3-dimethylindoline-1-yl-2-ylidene))bis(prop-1-en-1-yl-3-ylidene))bis(3,3-dimethyl-3H-indole-1-ium-2,1-diyl))bis(butanoyl))bis(butylazanediyl))bis(propane-1-sulfonate) **(BTF-2).**

Cyanine 3 NHS ester (**II**) (60 mg, 0.08 mmol) was dissolved in abs. DMF (200 µL) in eppendorf tube. L-lysine hydrochloride (5.5 mg, 0.03 mmol) was dissolved in 0.2 mM TEAA buffer pH = 8.25 (200

μL) and added to the NHS ester in DMF. The vessel was plugged, wrapped with parafilm and agitated at Thermomix shaker at +40°C. Reaction conversion was monitored with RP-HPLC on C18 reversed phase silica gel. After 12 h reaction mixture without any work up was applied onto a C18 silica gel column equilibrated with eluent A: miliQ water + 0.5 v/v% of acetic acid and gradually eluted to eluent B: miliQ water/acetonitrile/acetic acid = 20:80:0.5 v/v/v%). Pure fractions were combined concentrated with rotovap to approx. 1/10 of the initial volume and the residue was lyophilized in vacuum to obtain red powder (20.8 mg, 46%). R_f = 0.59 (DCM/MeOH/H_2O/AcOH = 84:15:1:0.2); ^{1}H NMR (400.13 MHz, chloroform-d) δ ppm: 8.54 (t, *J* = 13.4 Hz, 2H), 8.06 (m, 0.4H, NH), 7.53 (m, 4H), 7.38-7.46 (m, 8H), 7.30 (m, 4H), 6.53-6.63 (m, 4H), 4.31 (m, 1H), 4.21 (m, 8H), 3.57 (m, 2H), 3.50 (t, *J* = 7.0 Hz, 2H), 3.34 (m, 2H), 3.18 (m, 2H), 2.86 (m, 4H), 2.69 (m, 2H), 2.59 (m, 2H), 2.52 (m, 2H), 2.47 (m, 2H), 2.10 (m, 12H), 1.88 (m, 2H), 1.76 (s, 24H), 1.51 (m, 8H), 1.30 (m, 6H), 0.92 (m, 6H); HRMS (ESI) m/z: [M+2H]/2 calcd. for $C_{82}H_{114}N_8O_{12}S_2^{2+}$: 733.3994; found: 733.4005.

3-(N-butyl-4-(2-((1E,3E)-5-((Z)-1-(4-((2,5-dioxopyrrolidin-1-yl)oxy)-4-oxobutyl)-3,3-dimethylindolin-2-ylidene)penta-1,3-dien-1-yl)-3,3-dimethyl-3H-indol-1-ium-1-yl)butanamido)propane-1-sulfonate (Cy5 NHS ester (**IV**)).
Cyanine 5 free carboxylic acid (**III**) (70 mg, 0.1 mmol) was dissolved in dry DCM (1 mL) followed by DIPEA (26 μL, 0.15 mmol) and TSTU (45 mg, 0.15 mmol). The reaction was kept with stirring at room temperature for 5 h and precipitated with diethyl ether (20 mL) and acetic acid (100 μL) mixture. Formed solid was separated by filtration, washed with ether (2×10 mL) and dried in vacuum desiccator. NHS ester of Cy5 derivative (70 mg, 90%) was obtained as blue solid and used directly in the next step without any further purification. HRMS (ESI) m/z: [M+H] calcd. for $C_{44}H_{57}N_4O_8S^+$: 801.3892; found: 801.3897.

3,3'-((4,4'-(((1E,1'E,3E,3'E)-((2Z,2'Z)-(((1-carboxypentane-1,5-diyl)bis(azanediyl))bis(4-oxobutane-4,1-diyl))bis(3,3-dimethylindoline-1-yl-2-ylidene))bis(penta-1,3-dien-1-yl-5-ylidene))bis(3,3-dimethyl-3H-indole-1-ium-2,1-diyl))bis(butanoyl))bis(butylazanediyl))bis(propane-1-sulfonate) **(BTF-3)**.

Cyanine 5 NHS ester (**IV**) (21.0 mg, 0.026 mmol) was dissolved in abs. DMF (100 μL) in an Eppendorf tube. L-lysine hydrochloride (1.8 mg, 0.01 mmol) was dissolved in 0.2 mM TEAA buffer pH = 8.25 (100 μL) and added to the NHS ester in DMF. The vessel was plugged, wrapped with parafilm and agitated at Thermomix shaker at +40°C. Reaction conversion was monitored with RP-HPLC on C18 reversed phase silica gel. After 12 h reaction mixture without any work up was concentrated with rotovap to 1/3 of the volume and applied onto a LH-20 (Sigma Aldrich) size-exclusion column (20mm×600mm) equilibrated with DCM/MeOH = 1:1 gel column in a minimal volume and eluted with the same DCM/MeOH mixture. Pure fractions were analyzed by silica gel TLC plate, combined and concentrated with rotovap to afford dark-blue solid compound (12.8 mg, 84%). R_f = 0.63 (DCM/MeOH/H_2O/AcOH = 84:15:1:0.2); ^{1}H NMR (400.13 MHz, MeOD) δ ppm: 8.32 (m, 0.2 H, NH), 8.22 (t, *J* = 13.1 Hz, 4H), 8.06 (m, 0.5H, NH), 7.45 (t, *J* = 6.7 Hz, 4H), 7.28-7.42 (m, 8H), 7.17-7.28 (m, 4H), 6.59-6.78 (m, 2H), 6.50 (m, 1H), 6.34 (m, 3 H), 4.40 (bs, 1H), 4.15 (bs, 8H), 3.51 (m, 5H), 3.22 (bs, 2H), 2.86 (m, 4H), 2.65 (t, *J* = 7.4 Hz, 2 H), 2.49 (m, 6H), 2.08 (m, 12H), 1.69 (2s, 24H), 1.52 (m, 9H), 1.29 (m, 9H), 0.92 (m, 8H); HRMS (ESI) m/z: [M+2H]/2 calcd. for $C_{86}H_{118}N_8O_{12}S_2^{2+}$: 759.4168; found: 759.4168 and [M+H] calcd. for $C_{86}H_{117}N_8O_{12}S_2^+$: 1516.8154; found: 1518.8182.

3D-PAINT and SM*d*M. 3D-PAINT and SM*d*M experiments were performed similar to that described before,[28] yet with the simplicity that no pulsed illuminations were used. COS-7 cells (University of California Berkeley Cell Culture Facility) were maintained in Dulbecco's Modified Eagle Medium supplemented with 10% fetal bovine serum and 1% non-essential amino acids. Two days prior to imaging, cells were plated onto 18-mm diameter glass coverslips that were pretreated with hot piranha solutions (H_2SO_4:H_2O_2 at 3:1). The coverslip was assembled with a live-cell imaging holder (CSC-18, Bioscience Tools), and the sample was mounted on a Nikon Eclipse Ti-E inverted fluorescence microscope. **BTF-1**, **BTF-2**, **BTF-3,** Nile Red (Acros Organics), and DiD (Invitrogen) were serially diluted into the imaging medium (Leibovitz's L-15 medium, Gibco 21083027) to a final concentration of ~4 nM. This medium was added to the sample and remained unchanged throughout imaging. 560 nm and 647 nm lasers were focused to the back focal plane of an oil-immersion objective lens (Nikon CFI Plan Apochromat λ 100x, numerical aperture: 1.45). By shifting the laser beam toward the edge, the exiting beam was slightly below the critical angle of refraction of the coverslip-sample interface, thus illuminating ~1 μm into the sample. The sample was continuously illuminated with the 560 nm (for **BTF-1**, **BTF-2**, and Nile Red) or the 647 nm (for **BTF-3** and DiD) lasers. Typical total laser powers that entered the objective lens were ~50 mW, corresponding to ~1 kW/cm^2 at the sample. Brightness under different illumination powers (12-76 mW) were further examined for Figure S31. Single-molecule images owing to the transient entrance of individual dye molecules into the membrane phase, and hence fluorescence switch-on, were continuously recorded in the wide-field using an EM-CCD camera (iXon Ultra 897, Andor) at ~110 frames per second (~9 ms exposure time per frame). For 3D localization, a cylindrical lens was inserted into the optical path to induce astigmatism, so that the recorded images were stretched in the horizontal and vertical directions for single molecules above and below the focal plane, respectively.[6] 50,000 to 1200,000 frames were typically collected in each run. The recorded single-molecule images were each super-localized;[3,6] the resultant positions and transient displacements in successive frames were utilized to construct 3D-PAINT for topology and SM*d*M images for local diffusivity, respectively, as described previously.[3,6,28,48] Single-molecule trajectories (Figure S31) were analyzed using the TrackMate plugin of Fiji.[56]

ASSOCIATED CONTENT

Supporting Information

Spectroscopy data: fluorescence emission and absorbance spectra; analytical data for the prepared compounds: HPLC profiles, HRMS and NMR spectra; additional characterizations of single-molecule behaviors; videos of single-molecule images and sequence of live-cell super-resolution microscopy images.

AUTHOR INFORMATION

Corresponding Author

andrey.klymchenko@unistra.fr, xuk@berkeley.edu

Author Contributions

‡These authors contributed equally.

Notes

The authors declare no competing financial interests.

ORCID

Ilya O. Aparin: 0000-0001-8818-485X

Rui Yan: 0000-0003-3391-133X

Rémi pelletier: 0000-0002-1065-1398

Ke Xu: 0000-0002-2788-194X

Andrey S. Klymchenko: 0000-0002-2423-830X

ACKNOWLEDGMENT

This work was supported by the European Research Council ERC Consolidator grant BrightSens 648528, and the National Science Foundation (CHE-1554717 and CHE-2203518). I.O.A. acknowledges support from Marie Curie post-doctoral research grant (H2020-MSCA-IF-2018, DNANanoProbes 846571) by the European Union.

REFERENCES

(1) Hell, S. W.; Wichmann, J. Breaking the diffraction resolution limit by stimulated-emission - stimulated-emission-depletion fluorescence microscopy. *Opt. Lett.* **1994**, *19*, 780-782.
(2) Betzig, E.; Patterson, G. H.; Sougrat, R.; Lindwasser, O. W.; Olenych, S.; Bonifacino, J. S.; Davidson, M. W.; Lippincott-Schwartz, J.; Hess, H. F. Imaging intracellular fluorescent proteins at nanometer resolution. *Science* **2006**, *313*, 1642-1645.
(3) Rust, M. J.; Bates, M.; Zhuang, X. W. Sub-diffraction-limit imaging by stochastic optical reconstruction microscopy (STORM). *Nat. Methods* **2006**, *3*, 793-795.
(4) Sahl, S. J.; Hell, S. W.; Jakobs, S. Fluorescence nanoscopy in cell biology. *Nat. Rev. Mol. Cell Biol.* **2017**, *18*, 685-701.
(5) Schermelleh, L.; Ferrand, A.; Huser, T.; Eggeling, C.; Sauer, M.; Biehlmaier, O.; Drummen, G. P. C. Super-resolution microscopy demystified. *Nature Cell Biology* **2019**, *21*, 72-84.
(6) Huang, B.; Wang, W.; Bates, M.; Zhuang, X. Three-dimensional super-resolution imaging by stochastic optical reconstruction microscopy. *Science* **2008**, *319*, 810-3.
(7) Sauer, M.; Hofkens, J.; Enderlein, J. *Handbook of fluorescence spectroscopy and imaging: from ensemble to single molecules*, 2012; Vol. 403.
(8) Dempsey, G. T.; Vaughan, J. C.; Chen, K. H.; Bates, M.; Zhuang, X. W. Evaluation of fluorophores for optimal performance in localization-based super-resolution imaging. *Nat. Methods* **2011**, *8*, 1027-1036.
(9) Wang, L.; Frei, M. S.; Salim, A.; Johnsson, K. Small-Molecule Fluorescent Probes for Live-Cell Super-Resolution Microscopy. *Journal of the American Chemical Society* **2018**, *141*, 2770-2781.
(10) Heilemann, M.; van de Linde, S.; Schüttpelz, M.; Kasper, R.; Seefeldt, B.; Mukherjee, A.; Tinnefeld, P.; Sauer, M. Subdiffraction-Resolution Fluorescence Imaging with Conventional Fluorescent Probes. *Angewandte Chemie International Edition* **2008**, *47*, 6172-6176.
(11) Grimm, J. B.; English, B. P.; Chen, J. J.; Slaughter, J. P.; Zhang, Z. J.; Revyakin, A.; Patel, R.; Macklin, J. J.; Normanno, D.; Singer, R. H.; Lionnet, T.; Lavis, L. D. A general method to improve fluorophores for live-cell and single-molecule microscopy. *Nat. Methods* **2015**, *12*, 244-250.
(12) Li, H. L.; Vaughan, J. C. Switchable Fluorophores for Single-Molecule Localization Microscopy. *Chem. Rev.* **2018**, *118*, 9412-9454.

(13) Dempsey, G. T.; Bates, M.; Kowtoniuk, W. E.; Liu, D. R.; Tsien, R. Y.; Zhuang, X. Photoswitching Mechanism of Cyanine Dyes. *Journal of the American Chemical Society* **2009**, *131*, 18192-18193.
(14) Heilemann, M.; van de Linde, S.; Mukherjee, A.; Sauer, M. Super-Resolution Imaging with Small Organic Fluorophores. *Angewandte Chemie International Edition* **2009**, *48*, 6903-6908.
(15) Zheng, Q.; Ayala, A. X.; Chung, I.; Weigel, A. V.; Ranjan, A.; Falco, N.; Grimm, J. B.; Tkachuk, A. N.; Wu, C.; Lippincott-Schwartz, J.; Singer, R. H.; Lavis, L. D. Rational Design of Fluorogenic and Spontaneously Blinking Labels for Super-Resolution Imaging. *ACS Central Science* **2019**, *5*, 1602-1613.
(16) Takakura, H.; Zhang, Y.; Erdmann, R. S.; Thompson, A. D.; Lin, Y.; McNellis, B.; Rivera-Molina, F.; Uno, S.-n.; Kamiya, M.; Urano, Y.; Rothman, J. E.; Bewersdorf, J.; Schepartz, A.; Toomre, D. Long time-lapse nanoscopy with spontaneously blinking membrane probes. *Nature Biotechnology* **2017**, *35*, 773-780.
(17) Uno, S. N.; Kamiya, M.; Yoshihara, T.; Sugawara, K.; Okabe, K.; Tarhan, M. C.; Fujita, H.; Funatsu, T.; Okada, Y.; Tobita, S.; Urano, Y. A spontaneously blinking fluorophore based on intramolecular spirocyclization for live-cell super-resolution imaging. *Nature Chemistry* **2014**, *6*, 681-689.
(18) Uno, K.; Aktalay, A.; Bossi, M. L.; Irie, M.; Belov, V. N.; Hell, S. W. Turn-on mode diarylethenes for bioconjugation and fluorescence microscopy of cellular structures. *Proceedings of the National Academy of Sciences* **2021**, *118*, e2100165118.
(19) Habuchi, S.; Ando, R.; Dedecker, P.; Verheijen, W.; Mizuno, H.; Miyawaki, A.; Hofkens, J. Reversible single-molecule photoswitching in the GFP-like fluorescent protein Dronpa. *Proc. Natl. Acad. Sci. U. S. A.* **2005**, *102*, 9511-9516.
(20) Geertsema, H. J.; Aimola, G.; Fabricius, V.; Fuerste, J. P.; Kaufer, B. B.; Ewers, H. Left-handed DNA-PAINT for improved super-resolution imaging in the nucleus. *Nat Biotechnol* **2021**, *39*, 551-554.
(21) Jungmann, R.; Avendano, M. S.; Woehrstein, J. B.; Dai, M. J.; Shih, W. M.; Yin, P. Multiplexed 3D cellular super-resolution imaging with DNA-PAINT and Exchange-PAINT. *Nat. Methods* **2014**, *11*, 313-U292.
(22) Jungmann, R.; Steinhauer, C.; Scheible, M.; Kuzyk, A.; Tinnefeld, P.; Simmel, F. C. Single-Molecule Kinetics and Super-Resolution Microscopy by Fluorescence Imaging of Transient Binding on DNA Origami. *Nano Letters* **2010**, *10*, 4756-4761.
(23) Sharonov, A.; Hochstrasser, R. M. Wide-field subdiffraction imaging by accumulated binding of diffusing probes. *Proceedings of the National Academy of Sciences* **2006**, *103*, 18911-18916.
(24) Bongiovanni, M. N.; Godet, J.; Horrocks, M. H.; Tosatto, L.; Carr, A. R.; Wirthensohn, D. C.; Ranasinghe, R. T.; Lee, J. E.; Ponjavic, A.; Fritz, J. V.; Dobson, C. M.; Klenerman, D.; Lee, S. F. Multi-dimensional super-resolution imaging enables surface hydrophobicity mapping. *Nature communications* **2016**, *7*, 13544.
(25) Moon, S.; Yan, R.; Kenny, S. J.; Shyu, Y.; Xiang, L. M.; Li, W.; Xu, K. Spectrally Resolved, Functional Super-Resolution Microscopy Reveals Nanoscale Compositional Heterogeneity in Live-Cell Membranes. *J. Am. Chem. Soc.* **2017**, *139*, 10944-10947.
(26) Yan, R.; Moon, S.; Kenny, S. J.; Xu, K. Spectrally Resolved and Functional Super-resolution Microscopy via Ultrahigh-Throughput Single-Molecule Spectroscopy. *Accounts of Chemical Research* **2018**, *51*, 697-705.
(27) Danylchuk, D. I.; Moon, S.; Xu, K.; Klymchenko, A. S. Switchable Solvatochromic Probes for Live‐Cell Super‐resolution Imaging of Plasma Membrane Organization. *Angew. Chem. Int. Ed.* **2019**, *58*, 14920-14924.
(28) Yan, R.; Chen, K.; Xu, K. Probing Nanoscale Diffusional Heterogeneities in Cellular Membranes through Multidimensional Single-Molecule and Super-Resolution Microscopy. *Journal of the American Chemical Society* **2020**, *142*, 18866-18873.
(29) García-Calvo, J.; Maillard, J.; Fureraj, I.; Strakova, K.; Colom, A.; Mercier, V.; Roux, A.; Vauthey, E.; Sakai, N.; Fürstenberg, A.; Matile, S. Fluorescent Membrane Tension Probes for Super-Resolution Microscopy: Combining Mechanosensitive Cascade Switching with Dynamic-Covalent Ketone Chemistry. *Journal of the American Chemical Society* **2020**, *142*, 12034-12038.
(30) Okamoto, A. ECHO probes: a concept of fluorescence control for practical nucleic acid sensing. *Chemical Society Reviews* **2011**, *40*, 5815-5828.
(31) Bouhedda, F.; Fam, K. T.; Collot, M.; Autour, A.; Marzi, S.; Klymchenko, A.; Ryckelynck, M. A dimerization-based fluorogenic dye-aptamer module for RNA imaging in live cells. *Nature Chemical Biology* **2020**, *16*, 69-76.

(32) Farzan, V. M.; Kvach, M. V.; Aparin, I. O.; Kireev, D. E.; Prikazchikova, T. A.; Ustinov, A. V.; Shmanai, V. V.; Shipulin, G. A.; Korshun, V. A.; Zatsepin, T. S. Novel homo Yin-Yang probes improve sensitivity in RT-qPCR detection of low copy HIV RNA. *Talanta* **2019**, *194*, 226-232.
(33) Esteoulle, L.; Daubeuf, F.; Collot, M.; Riche, S.; Durroux, T.; Brasse, D.; Marchand, P.; Karpenko, I. A.; Klymchenko, A. S.; Bonnet, D. A near-infrared fluorogenic dimer enables background-free imaging of endogenous GPCRs in living mice. *Chemical Science* **2020**, *11*, 6824-6829.
(34) Fam, K. T.; Collot, M.; Klymchenko, A. S. Probing biotin receptors in cancer cells with rationally designed fluorogenic squaraine dimers. *Chemical Science* **2020**, *11*, 8240-8248.
(35) Karpenko, I. A.; Collot, M.; Richert, L.; Valencia, C.; Villa, P.; Mely, Y.; Hibert, M.; Bonnet, D.; Klymchenko, A. S. Fluorogenic Squaraine Dimers with Polarity-Sensitive Folding As Bright Far-Red Probes for Background-Free Bioimaging. *Journal of the American Chemical Society* **2015**, *137*, 405-412.
(36) Klymchenko, A. S. Solvatochromic and Fluorogenic Dyes as Environment-Sensitive Probes: Design and Biological Applications. *Acc. Chem. Res.* **2017**, *50*, 366-375.
(37) Lew, M. D.; Lee, S. F.; Ptacin, J. L.; Lee, M. K.; Twieg, R. J.; Shapiro, L.; Moerner, W. E. Three-dimensional superresolution colocalization of intracellular protein superstructures and the cell surface in live *Caulobacter crescentus*. *Proc. Natl. Acad. Sci. U. S. A.* **2011**, *108*, E1102-E1110.
(38) Sezgin, E.; Levental, I.; Mayor, S.; Eggeling, C. The mystery of membrane organization: composition, regulation and roles of lipid rafts. *Nat. Rev. Mol. Cell Biol.* **2017**, *18*, 361-374.
(39) Lingwood, D.; Simons, K. Lipid Rafts As a Membrane-Organizing Principle. *Science* **2010**, *327*, 46-50.
(40) Simons, K.; Ikonen, E. Functional rafts in cell membranes. *Nature* **1997**, *387*, 569-572.
(41) Johnson, M. E.; Berk, D. A.; Blankschtein, D.; Golan, D. E.; Jain, R. K.; Langer, R. S. Lateral diffusion of small compounds in human stratum corneum and model lipid bilayer systems. *Biophys. J.* **1996**, *71*, 2656-2668.
(42) Bacia, K.; Scherfeld, D.; Kahya, N.; Schwille, P. Fluorescence correlation spectroscopy relates rafts in model and native membranes. *Biophys J* **2004**, *87*, 1034-43.
(43) Nishimura, S. Y.; Lord, S. J.; Klein, L. O.; Willets, K. A.; He, M.; Lu, Z.; Twieg, R. J.; Moerner, W. E. Diffusion of lipid-like single-molecule fluorophores in the cell membrane. *J. Phys. Chem. B* **2006**, *110*, 8151-8157.
(44) Shim, S.-H.; Xia, C.; Zhong, G.; Babcock, H. P.; Vaughan, J. C.; Huang, B.; Wang, X.; Xu, C.; Bi, G.-Q.; Zhuang, X. Super-resolution fluorescence imaging of organelles in live cells with photoswitchable membrane probes. *Proceedings of the National Academy of Sciences* **2012**, *109*, 13978-13983.
(45) Hestand, N. J.; Spano, F. C. Expanded Theory of H- and J-Molecular Aggregates: The Effects of Vibronic Coupling and Intermolecular Charge Transfer. *Chemical Reviews* **2018**, *118*, 7069-7163.
(46) Davis, M. M.; Helzer, H. B. Titrimetric and equilibrium studies using indicators related to nile blue A. *Anal. Chem.* **1966**, *38*, 451-461.
(47) Cser, A.; Nagy, K.; Biczók, L. Fluorescence lifetime of Nile Red as a probe for the hydrogen bonding strength with its microenvironment. *Chem. Phys. Lett.* **2002**, *360*, 473-478.
(48) Xiang, L.; Chen, K.; Yan, R.; Li, W.; Xu, K. Single-molecule displacement mapping unveils nanoscale heterogeneities in intracellular diffusivity. *Nat. Methods* **2020**, *17*, 524-530.
(49) Xie, X. S.; Choi, P. J.; Li, G. W.; Lee, N. K.; Lia, G. Single-molecule approach to molecular biology in living bacterial cells. *Ann. Rev. Biophys.* **2008**, *37*, 417-444.
(50) Mockl, L.; Pedram, K.; Roy, A. R.; Krishnan, V.; Gustavsson, A. K.; Dorigo, O.; Bertozzi, C. R.; Moerner, W. E. Quantitative Super-Resolution Microscopy of the Mammalian Glycocalyx. *Dev. Cell* **2019**, *50*, 57-72.
(51) Fam, K. T.; Saladin, L.; Klymchenko, A. S.; Collot, M. Confronting molecular rotors and self-quenched dimers as fluorogenic BODIPY systems to probe biotin receptors in cancer cells. *Chemical Communications* **2021**, *57*, 4807-4810.
(52) Shulov, I.; Rodik, R. V.; Arntz, Y.; Reisch, A.; Kalchenko, V. I.; Klymchenko, A. S. Protein-Sized Bright Fluorogenic Nanoparticles Based on Cross-Linked Calixarene Micelles with Cyanine Corona. *Angew Chem Int Ed Engl* **2016**, *55*, 15884-15888.
(53) Sakai, K.; Kaji, M.; Takamatsu, Y.; Tsuchiya, K.; Torigoe, K.; Tsubone, K.; Yoshimura, T.; Esumi, K.; Sakai, H.; Abe, M. Fluorocarbon–hydrocarbon gemini surfactant mixtures in aqueous solution. *Colloids and Surfaces A: Physicochemical and Engineering Aspects* **2009**, *333*, 26-31.

(54) Arbeloa, F. L.; Ojeda, P. R.; Arbeloa, I. L. Flourescence self-quenching of the molecular forms of Rhodamine B in aqueous and ethanolic solutions. *Journal of Luminescence* **1989**, *44*, 105-112.
(55) Texier, I.; Goutayer, M.; Da Silva, A.; Guyon, L.; Djaker, N.; Josserand, V.; Neumann, E.; Bibette, J.; Vinet, F. Cyanine-loaded lipid nanoparticles for improved in vivo fluorescence imaging. *Journal of Biomedical Optics* **2009**, *14*, 054005.
(56) Tinevez, J. Y.; Perry, N.; Schindelin, J.; Hoopes, G. M.; Reynolds, G. D.; Laplantine, E.; Bednarek, S. Y.; Shorte, S. L.; Eliceiri, K. W. TrackMate: An open and extensible platform for single-particle tracking. *Methods* **2017**, *115*, 80-90.

TOC Graphic